Int. J. Electrochem. Sci., 14 **(2019)** 3095 – 3113, doi: 10.20964/2019.03.07

International Journal of
ELECTROCHEMICAL
SCIENCE
www.electrochemsci.org

Electrochemical Behavior of ZE41 Magnesium Alloy under Simulated Atmospheric Corrosion

Linlin Nie[1], *Xuyang Zhao*[2], *Pan Liu*[1], *Lulu Hu*[1], *Jianqing Zhang*[1], *Jiming Hu*[1], *Fangfang Wu*[2], *Fahe Cao*[1,*]

[1] Department of Chemistry, Zhejiang University, Hangzhou 310027, China,
[2] Key Laboratory for Protection Technology of High-Rise Operation, Zhejiang Huadian Equipment Testing Institute Co. LTD, Hangzhou 310015, China
[*]E-mail: nelson_cao@zju.edu.cn

Received: 5 November 2018 / *Accepted:* 27 December 2018 / *Published:* 7 February 2019

The electrochemical measurement technology such as cathodic polarization curves, electrochemical impedance spectroscopy (EIS) and electrochemical noise (EN) were used to study the corrosion behavior of ZE41 magnesium alloy in bulk solution and under thin electrolyte layers (TELs) containing 3.5 wt. % NaCl. The electrochemical results indicate that the corrosion resistance of ZE41 under the TELs is enhanced compared to that in bulk solution. Moreover, in bulk solution uniform corrosion preferentially occurs and with the immersion time localized corrosion also arises, while under the TELs localized corrosion is the primary corrosion form which occupies higher ratio compared to uniform corrosion and with the thinning of the TELs and increasing of immersing time the ratio becomes higher.

Keywords: ZE41 Magnesium Alloy; EIS; Electrochemical Noise; TEL; Corrosion Resistance; Corrosion Form.

1. INTRODUCTION

In the 21st century, lightweight materials industries developed rapidly for the pressure of energy saving and environmental protection. Some studies indicated that the utilization rate of fuel in the internal combustion engine increase 6% to 8% once the car weight reduces 10% and as a result magnesium and its alloy gained widespread attention as the lightest metal structural materials in the world [1,2]. Moreover, magnesium alloy revealed high specific intensity, electromagnetic shielding properties and etc. [3,4], which is potentially alternative metal material for working aloft. Many researches have been conducted aiming at the poor corrosion resistance of magnesium and its alloy [5,6,7,8,9,10,11].

For the study of ZE41 magnesium some researches have been reported. The study of Johnston has analyzed and compared the corrosion rate of high pure magnesium, AZ91 magnesium alloy and ZE41 magnesium alloy in bicarbonate buffer solution [12]. The result indicated that the corrosion rate of ZE41 was the highest and the corrosion resistance of high pure magnesium was a little higher than that of AZ91. Besides, more stable surface films were formed on those three metals and the corrosion rate of them decreased with the rising of the solution pH. Taltavull of the research group [13] also studied the effect of the conentration of Cl^- to the corrosion of that three metals, which manifested that the concentration of Cl^- effected the corrosion behavior through the influence on protectiveness of surface film, the intensity of the micro thermocouple formed and the corrosion morphology. In details, for the concentration of 0 M, the corrosion rate of high pure magnesium is the highest, while for the concentration of 0.1, 0.14, 0.3 and 1 M of chloride ion, pitting corrosion appeared for the Cl^- reduced the protectiveness of surface film, so galvanic corrosion happened in magnesium alloy, which resulted in the corrosion rate of AZ91, ZE41 and high pure magnesium decreasing in turn. Chakraborty Banerjee [14] researched the corrosion behavior of laser surface melted ZE41 magnesium alloy in 0.001 M NaCl, which showed that the laser surface melted ZE41 consisted of equiaxed columnar grains and intermetallic particles distributed along the grain boundaries formed a continuous network like structure. The intermetallic particles had a highly refined structure with the grain size from 1 to 5 µm, which was obvious smaller than the size of untreated ZE41 (about 50 µm). Although laser surface melted ZE41 shows highly refined microstructure, it is different to the corrosion behavior of AZ series magnesium alloys that laser surface melting did not significantly improve the corrosion resistance of ZE41. The phenomenon is due to the absence of beneficial alloying elements such as Al.

The corrosion behavior of ZE41 magnesium alloy in bulk solution has been widely studied. As well known, most of the usage environment of these alloys is exposed in the atmosphere. However, the researches in aggressive atmosphere have been little reported yet. So, the current research focuses on the corrosion behavior of ZE41 in simulate atmosphere condition namely under TELs in 3.5 wt. % NaCl solution is really necessary. Through the electrochemical technologies of cathodic curves, EIS and EN, combined with physical characterization, the corrosion resistance and corrosion type in bulk solution and under different TELs were investigated.

2. EXPERIMENTAL

Specimens used in the current research were commercial ZE41 magnesium alloy plates. The ZE41 ingots were cut into cylindrical electrodes and then the electrodes were sealed with nylon. For the measurements of EIS and cathodic polarization curves the diameter of the working electrode area was 4 mm, while for the electrochemical noise measurements a pair of identical ZE41 alloy electrodes with the diameter of 3 mm and in parallel with 2 mm apart, acting as the working and counter electrodes respectively, as displayed in the former paper [15]. The working electrode surface was mechanically grounded gradually by SiC papers through 400 to 1000 grades, polished with 1.0 µm Al_2O_3 powder, rinsed with distilled water, degreased with acetone, and then dried in a cool air flow.

The EIS at open circuit potential (OCP) under TELs were measured through VMP2 multichannel potentiostat (PARC, USA) with the amplitude of 5 mV of AC voltage and the frequency ranging from 100 kHz to 10 mHz. The cathodic polarization curves were obtained by the CHI630 potentiostat (Shanghai CH Instruments, Inc., China) with the potential sweep rate of 0.5 mV/s and potentials varying from the OCP to -0.4 V vs OCP. Both the EIS and the cathodic curves tests were measured by the traditional three electrode system (a large area of platinum wire as the counter electrode and the saturated calomel reference electrode). The electrochemical noise logs under TELs were controlled by a low noise potentiostat/galvanostat (Gamry PCI/4-G300, USA) with ZRA (zero resistance ammeter). Once the electrodes immersing into the 3.5 wt. % NaCl solution, the ESA410 software synchronously collected the fluctuations of the current and potential during initial 24 hours.

The experimental device simulating the atmospheric environment and the determination of thickness of TEL was designed by our group [**Error! Bookmark not defined.**] and the analysis of the electrochemical noise data have been introduced in detail in our previous work published in this journal [**Error! Bookmark not defined.**]. All of the experimental chemical reagents were analytically pure and the solutions were prepared by distilled water. The tests were conducted at room temperature.

3. RESULTS AND DISCUSSION

3.1 Cathodic polarization behavior

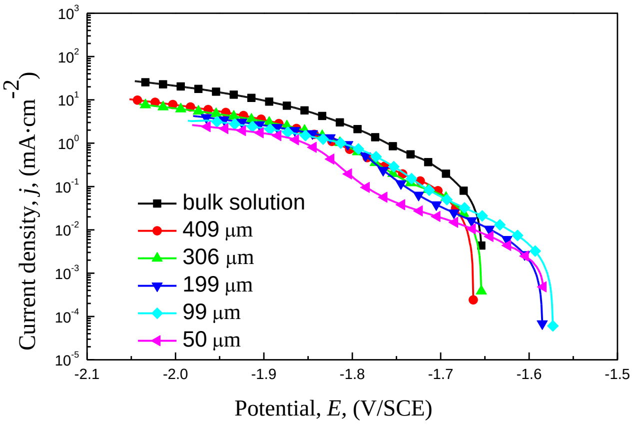

Figure 1. Cathodic polarization curves for ZE41 magnesium alloy under bulk solution and the given thicknesses of TEL containing 3.5 wt. % NaCl.

Polarization curve is most fundamental electrochemical method for studying the kinetics of electrode process, through which we could infer the characteristic and the rate determining step of the electrode reaction, determine the exchange current density and corrosion potential, measure the transfer coefficient and etc. Fig. 1 displays the cathodic polarization curves of ZE41 in bulk solution and under different TEL thicknesses. The Fig. 1 shows that all the curves have the similar shape, which is made of weak polarization region adjacent to the corrosion potential and the Tafel region. The phenomenon means that ZE41 shows similar electrode reaction mechanism of electrode process in bulk solution and the different TELs thicknesses. From the figure we can conclude that the cathodic current density in bulk solution is higher than that under TELs and the corrosion potential in bulk solution and under the TELs of 409 and 306 μm are obviously lower than that the TELs of 199, 99 and 50 μm.

According to theoretical knowledge in the electrode process of metal corrosion, when the electrode process is under the control of electrochemistry the relationship between potential and current density j can be expressed by the Eq. 1. When the process is under the Tafel region, the Eq. 1 can be simplified to the Eq. 2 with the anodic section removed.

$$j = j_{corr}\left[e^{\frac{E-E_{corr}}{\beta\alpha}} - e^{\frac{E-E_{corr}}{\beta c}}\right] \text{................................} [1]$$

$$j = j_{corr}\left[-e^{\frac{E-E_{corr}}{\beta c}}\right] \text{................................} [2]$$

Combined the Eq. 2 with the Tafel extrapolation method, the specific kinetic parameters obtained is displayed in Table 1. The parameter E_{corr} means the corrosion potential, j_{corr} means corrosion current density, β_c is the cathodic Tafel slop. It is obvious that j_{corr} in bulk solution (0.103 mA·cm^{-2}) is much higher than that under the TELs. j_{corr} decreases with the decrease of the TELs, for instance, under the TELs of 409 and 306 μm, j_{corr} is in the 10^{-2} mA·cm^{-2} orders of magnitude, while the thickness of TELs is thinner than 200 μm, j_{corr} is in the 10^{-3} mA·cm^{-2} orders of magnitude. In current research compared to bulk solution and thicker TELs thickness the j_{corr} under 200 μm sharply reduces, so the thickness of 200 μm is regarded as the critical thickness of TEL. Also, it is known that E_{corr} shifts to higher values with the thinning of the thickness of the TELs. As reported before [**Error! Bookmark not defined.**], the cathodic process of magnesium alloy corrosion in neutral sodium chloride solution is mainly controlled by reduction process of hydrated proton. Thus, in bulk solution, the products of electrode reactions can leave the electrode surface through diffusion and H_3O^+ can also transfer from bulk solution to the electrode surface. However, diffusion process is suppressed under the TELs, thus the concentration of H_3O^+ needed for cathodic reaction reduces and that of OH^- around the electrode surface increases. Some studies [16] indicate that it is benefit to the deposition of Mg^{2+} produced by anodic reactions at pH>9. The deposition forms corrosion product film on the electrode surface, which inhibits the anodic process of magnesium alloy corrosion by covering the sites of anodic reaction. To sum up, comparing to bulk solution the anodic and cathodic reactions of ZE41 magnesium alloy under the TELs are both inhibited, so the corrosion resistance enhances.

Table 1. Results obtained from cathodic polarization curves for ZE41 in bulk solution and the given thicknesses of TEL at exposure time of 1 h.

Thickness	**Bulk solution**	**409 μm**	**306 μm**	**199 μm**	**99 μm**	**50 μm**
E_{corr} (V vs SCE)	-1.653	-1.663	-1.653	-1.581	-1.59	-1.583
j_{corr} (mA·cm^{-2})	0.103	0.0353	0.0139	0.00333	0.00359	0.00288
β_c (mV·dec^{-1})	109.5	107.0	86.4	97.3	88.1	142.9

3.2 EIS behavior

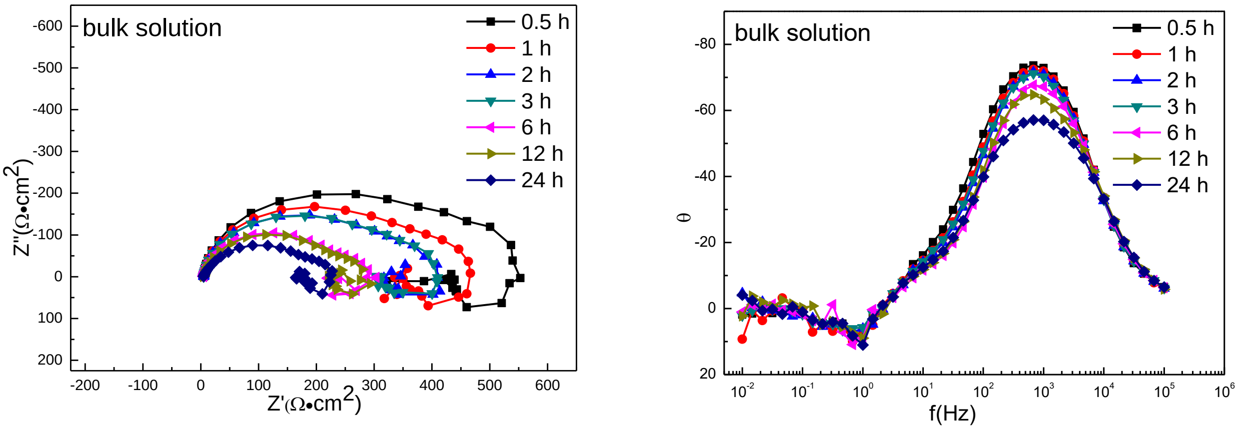

Figure 2. Experimental Nyquist and Bode plots of ZE41 magnesium alloy in bulk solution during 24 h immersion.

EIS is a powerful method to study the corrosion mechanism and the surface film of metal. The surface film formed once magnesium alloy immersing into 3.5 wt. % NaCl solutions is composed of two incompact layers which are the inner layer of MgO attached to metal surface and the porous outer layer of hydroxide [17].

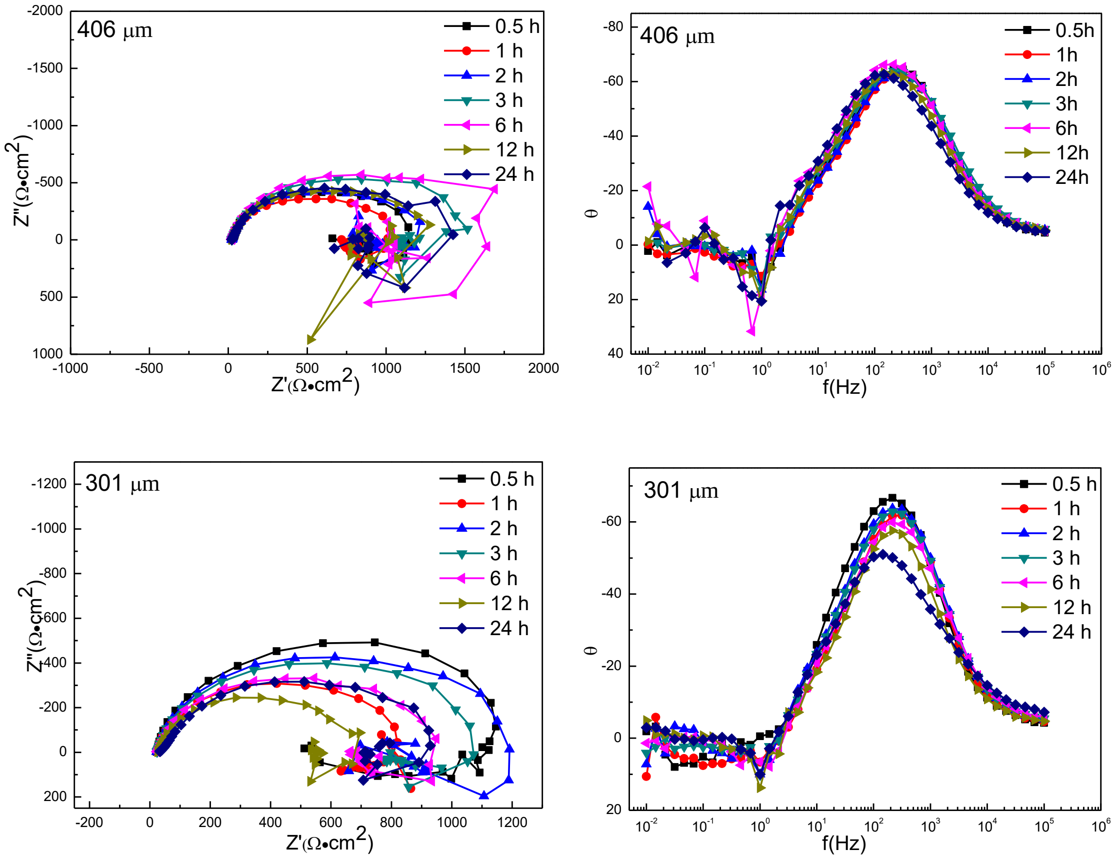

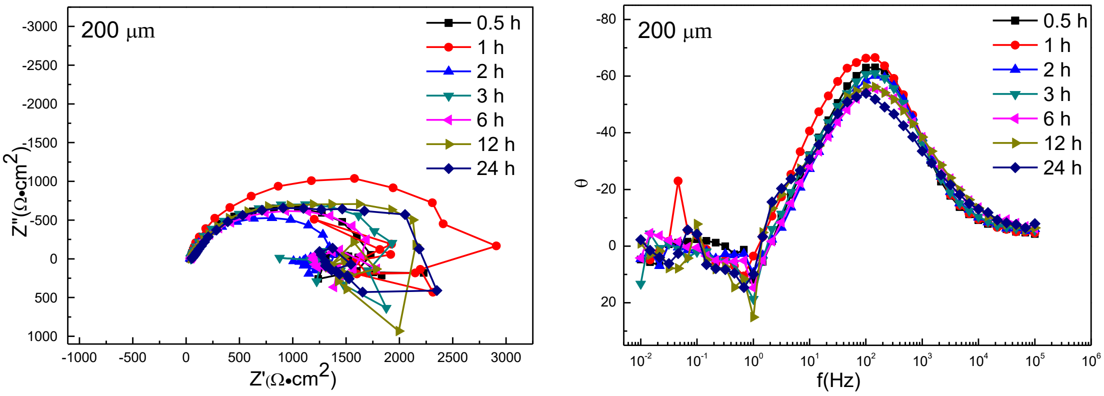

Figure 3. Experimental Nyquist and Bode plots of ZE41 under some given thicknesses (406, 301 and 200 μm) of TEL during 24 h immersion.

In the current research, the equivalent circuit model is used to study corrosion behavior of ZE41 in bulk solution and under TELs, including the the impedance of charge transfer, surface film and so on.

Fig. 2 shows the Nyquist and Bode curves of ZE41 immersing in 3.5 wt. % NaCl bulk solutions during 24 hours. The EIS plots indicate that all Nyquist curves consist of two overlapped capacitive arcs at high and intermediate frequency region and an inductive arc at low frequency region, which is similar to the phenomenon other researchers have been observed [10,18,19]. From Fig. 3 and Fig. 4, it is known that the shape and change trend of EIS with immersion time under the TELs are similar with that in bulk solution, meanwhile the partly overlapped capacitive reactance arcs at high and intermediate frequency region under the TELs is bigger than that in bulk solution. Combined with the previous research of AZ91D magnesium alloy and our previous work [10], the capacitive reactance arcs at high frequency area relate to the mass transfer process of ions through the surface film and the diameter of capacitive reactance arcs at intermediate frequency region depends on the charge transfer resistance. The impedance behavior at low frequency region (<1.46 Hz) is considered to the adsorption of active surface particles (eg. Mg_{ads}^{+}) [20,21].

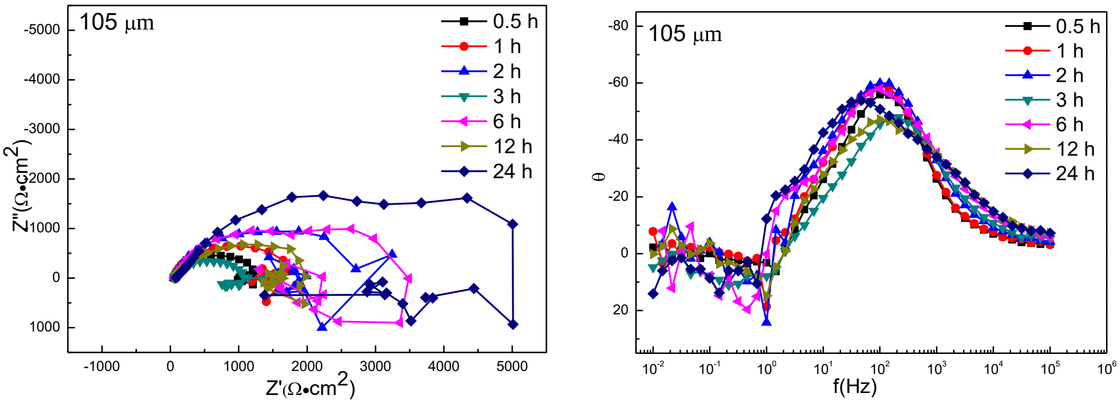

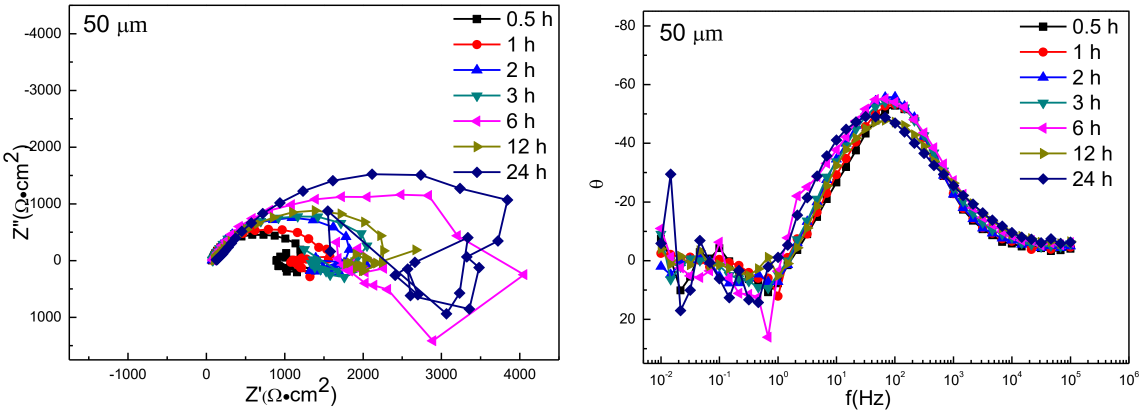

Figure 4. Experimental Nyquist and Bode plots of ZE41 under the TELs thicknesses of 105 and 50 μm during 24 h immersion.

To better understanding the corrosion kinetic course of ZE41, the equivalent circuit including three time constants shown in Fig. 5 is used to simulate the data of EIS. In this equivalent circuit the charge transfer process of double electrode layer and the surface film of corrosion products are mainly considered. In details, R_s is solution resistance, the value of R_t means charge transfer resistance, C_{dl} represents the capacitance of electric double layer. Moreover, R_t and C_{dl} in parallel indicate the Faraday process characteristics of the double layer between metal and the surface film. Nevertheless, due to the dispersion effect revealed in the Nyquist plots, C_{dl} in the equivalent circuit is replaced by CPE_{dl} [18]. R_{surf} explains the resistance of the surface film forming on ZE41, whose value mainly depends on the porous degree of the surface film and the electro conductibility of solution through the microspores of the surface film. Constant phase element CPE_{surf} in parallel with R_{surf} indicate the capacitance of the surface film, the value of which is in direct proportion to the porosity and inverse proportion to the thickness of the surface film [21]. R_{Mg+} and L_{Mg+} indicate the inductive reactance and impedance value of the active intermediate in the process of electrochemical process. Under the TELs the data are so dispersed that it is hard to obtain accurate value of R_{Mg+} and L_{Mg+}, besides, the information of R_{Mg+} and L_{Mg+} are not contained at high and intermediate frequency area, so in actual simulation the values of R_{Mg+} and L_{Mg+} are not adopted.

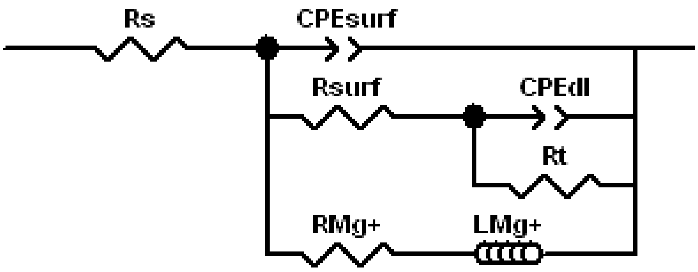

Figure 5. Equivalent circuit model of ZE41 magnesium alloy for EIS in 3.5 wt. % NaCl solutions.

Table 2. Fitting results obtained from equivalent circuit for ZE41 under bulk solution and different TELs.

Thickness (μm)	Time (h)	R_s ($\Omega\cdot cm^2$)	CPE_{surf} ($\mu F\cdot cm^{-2}\cdot Hz^{1-n1}$)	n_1	R_{surf} ($\Omega\cdot cm^2$)	CPE_{dl} ($\mu F\cdot cm^{-2}\cdot Hz^{1-n2}$)	n_2	R_t ($\Omega\cdot cm^2$)	$R_{surf}+R_t$ ($\Omega\cdot cm^2$)
Bulk solution	0.5	5.07	7.64	0.95	427.84	107.46	1	115.00	542.85
	1	5.08	7.99	0.95	366.39	156.86	1	90.76	457.14
	2	5.05	8.61	0.94	325.94	195.56	1	74.55	400.49
	3	4.70	9.63	0.93	328.88	203.21	1	72.94	401.83
	6	4.84	10.69	0.92	238.56	364.15	1	45.38	283.94
	12	4.58	16.60	0.88	244.06	743.93	1	32.02	276.08
	24	4.60	30.30	0.82	199.29	768.68	1	24.33	223.62
407 μm	0.5	22.80	8.20	0.92	556.26	86.58	1	157.90	714.16
	1	23.11	8.61	0.90	771.65	58.06	1	216.77	988.42
	2	21.48	10.34	0.89	737.29	86.07	1	190.09	927.38
	3	23.29	10.54	0.89	527.79	80.98	1	112.13	639.92
	6	23.37	11.97	0.88	532.89	121.72	1	113.41	646.30
	12	24.37	15.53	0.87	380.33	234.78	1	59.83	440.16
	24	27.17	30.56	0.77	70.39	1.49	1	381.70	452.09
301 μm	0.5	23.44	9.57	0.91	1043.60	44.31	1	139.60	1183.20
	1	23.64	10.13	0. 90	717.85	96.77	1	95.46	813.32
	2	23.97	10.29	0.88	1034.57	117.65	1	129.77	1164.33
	3	24.13	11.25	0.88	986.07	146.17	1	78.46	1064.53
	6	24.76	14.16	0.84	849.21	1.80	1	64.50	913.71
	12	24.62	13.95	0.79	10.84	3.56	0.96	640.29	651.13
	24	31.57	11.31	0.77	33.93	10.64	0.82	898.69	932.62
197 μm	0.5	35.99	12.32	0.87	999.03	124.78	1	109.98	1109.00
	1	38.27	13.65	0.86	732.78	16.04	1	53.78	786.56
	2	40.39	14.51	0.84	925.00	134.96	1	76.05	1001.05
	3	35.13	11.31	0.70	15.87	7.79	0.86	1144.33	1160.2
	6	37.88	9.32	0.75	19.57	9.22	0.82	873.56	893.13
	12	40.35	8.86	0.78	29.00	14.41	0.75	1067.55	1096.55
	24	40.06	7.54	0.73	19.85	24.45	0.70	966.24	986.09
105 μm	0.5	59.49	12.12	0.88	1106.63	137.0	1	83.88	1190.51
	1	59.69	12.02	0.87	1578.26	104.91	1	128.43	1706.69
	2	60.40	11.92	0.84	2404.3	62.64	1	272.93	2677.23
	3	51.78	7.03	0.73	17.3	10.13	0.81	1017.29	1034.58
	6	62.05	15.38	0.76	2991.39	171.12	1	475.36	3466.75
	12	66.80	11.71	0.74	273.12	5.76	0.79	1808.18	2081.31
	24	77.85	15.74	0.70	646.19	1.25	0.98	4820.19	5466.37
50 μm	0.5	65.89	11.76	0.73	16.21	6.06	0.93	1207.94	1224.15
	1	68.02	4.75	0.78	17.46	9.88	0.88	1434.53	1452.0

	2	72.63	4.77	0.8	19.63	8.81	0.88	1897.92	1917.55
	3	75.40	3.16	0.82	20.17	11.10	0.83	2102.71	2122.87
	6	75.69	6.47	0.7	27.45	10.19	0.81	3437.30	3464.75
	12	99.82	6.21	0.79	102.87	7.79	0.81	2297.09	2399.96
	24	125.01	9.07	0.75	212.84	6.21	0.80	4237.42	4450.26

Table 2 shows the fitting results of EIS data, in which the significance of R_s, R_{surf}, R_t, CPE_{surf} and CPE_{dl} are the same as that described in Fig. 5. Meanwhile, n, an index of dimensionless, is the parameter of CPE, which is equal to equivalent resistance at n=0, equivalent capacitance at n=1 and equivalent inductance at n=-1. In Table 2, the value of R_s in bulk solution is about 5 $\Omega\cdot cm^2$, which is much smaller than that under the TELs and shows no obvious fluctuation with the extension of immersion time. Under the TELs the value of R_s increases with the decrease of the TELs and with the extension of immersion time, for example, R_s under 407 μm increases from 22.8 $\Omega\cdot cm^2$ to 27.17 $\Omega\cdot cm^2$ with immersing time. Moreover, R_s value under 50 μm fluctuates but not always increases at the range of 65.89 to 125.01 $\Omega\cdot cm^2$ at during test time mainly because of the deposition of non-conductive corrosion products on the electrode surface with the immersing time. Some researches pointed out that the value of R_t is inversely proportional to corrosion rate [18,22]. Other research indicated that corrosion resistance is also relation to the properties of surface film, namely, compact and thick film can protect the metallic matrix through reducing the anodic reacton sites and impeding the diffusion of corrosion products [23]. In addition, it is known in this study the time constants in high and immediate frequency area are not easy to distinguish, so the sum of R_{surf} and R_t ($R_{surf}+R_t$) is used to character the change of corrosion resistance. Fig. 6 displays the change of (R_{surf}+R_t) with the time in bulk solution and under various TELs. It is obvious from Fig. 6 that (R_{surf}+R_t) under TELs is bigger than in bulk solution and gradually increase with thinning of the TELs, which suggests that the corrosion resistance is higher under the TELs than that in bulk solution and increases with the thinning of the TELs. Besides, the corrosion of ZE41 can be divided to three groups on the basis of the change of corrosion resistance with time. In bulk solution, the corrosion resistance continually decreases from 542.85 to 223.62 $\Omega\cdot cm^2$ with the immersion time. The corrosion resistance firstly increases and then decreases under the TELs of 407, 301 and 200 μm. Under the TELs of 105 and 50 μm, the corrosion resistances progressively increase during the time of 0-3 h and 0-6 h respectively, then still shows increasing trend on the whole but fluctuation severely with the time of immersion. As known from the polarization curves, no matter in bulk solution or under the TELs of 3.5wt% NaCl the cathodic reaction of ZE41 is the reduction of hydronium ion. The reasons of the different experiment results can be explained as follows: firstly, when the electrode immerses into bulk solution, the positive ions produced can diffuse to bulk solution timely and as the extension of immersion time the area of matrix exposed in solution increases with the oxidation film formed in air gradually brakes under the role of Cl^-, so the corrosion rate increase with immersion time. Secondly, under relatively thick TELs (407, 301 and 200 μm), some of the produced Mg^{2+} cannot diffuse to bulk solution timely which will combine with OH^- produced on the electrode surface through the cathodic reaction. These combinations on one hand can increase the metal corrosion resistance; on the other hand, Cl^- could intrude into the matrix because of their porosity in nature with time which promotes the further dissolution of the electrode. Thirdly, under very thin TELs (105 and 50 μm in our case), the diffusion of Mg^{2+} is severely inhibited and the concentration of OH^- is high, thus resulting in the deposition of corrosion products on the electrode surface. Furthermore, the concentration of H_3O^+ on the electrode surface decreases and the cathodic reaction is also restrained. So under very thin TELs, the corrosion resistance increases by a large margin and stains the growth trend on the whole with time. The corrosion resistances under the TELs of 105 and 50 μm fluctuate remarkably. Combined with electrochemical noise data the phenomenon is mainly attributed to the domination of localized corrosion as discussed below.

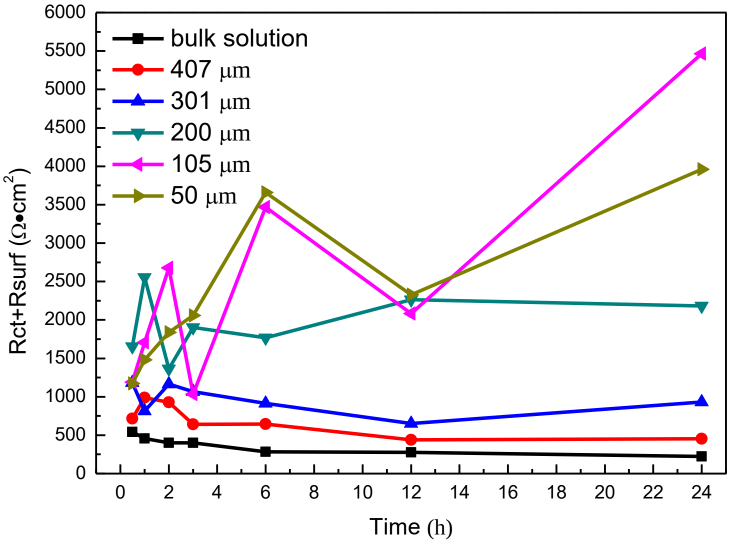

Figure 6. R_{surf}+R_t results of ZE41 alloy in bulk solution and under given thicknesses TEL during immersion in 3.5 wt. % NaCl solutions.

3.3 Electrochemical noise behavior

Electrochemical noise technique shows two prominent advantages than other traditional electrochemical methods. On the one hand, it is a kind of in-situ nondestructive electrochemical measurement technology, so there is no need to add any extra disturbing signal which may affect the study system during the experiment [24,25]. On the other hand, electrochemical noise signal and analysis can provide the information of corrosion rate and mechanism synchronously [26]. The fluctuant amplitude of current and potential on the time domain plot can reflect the corrosion intensity and the fluctuant shape is related to the corrosion type [27].

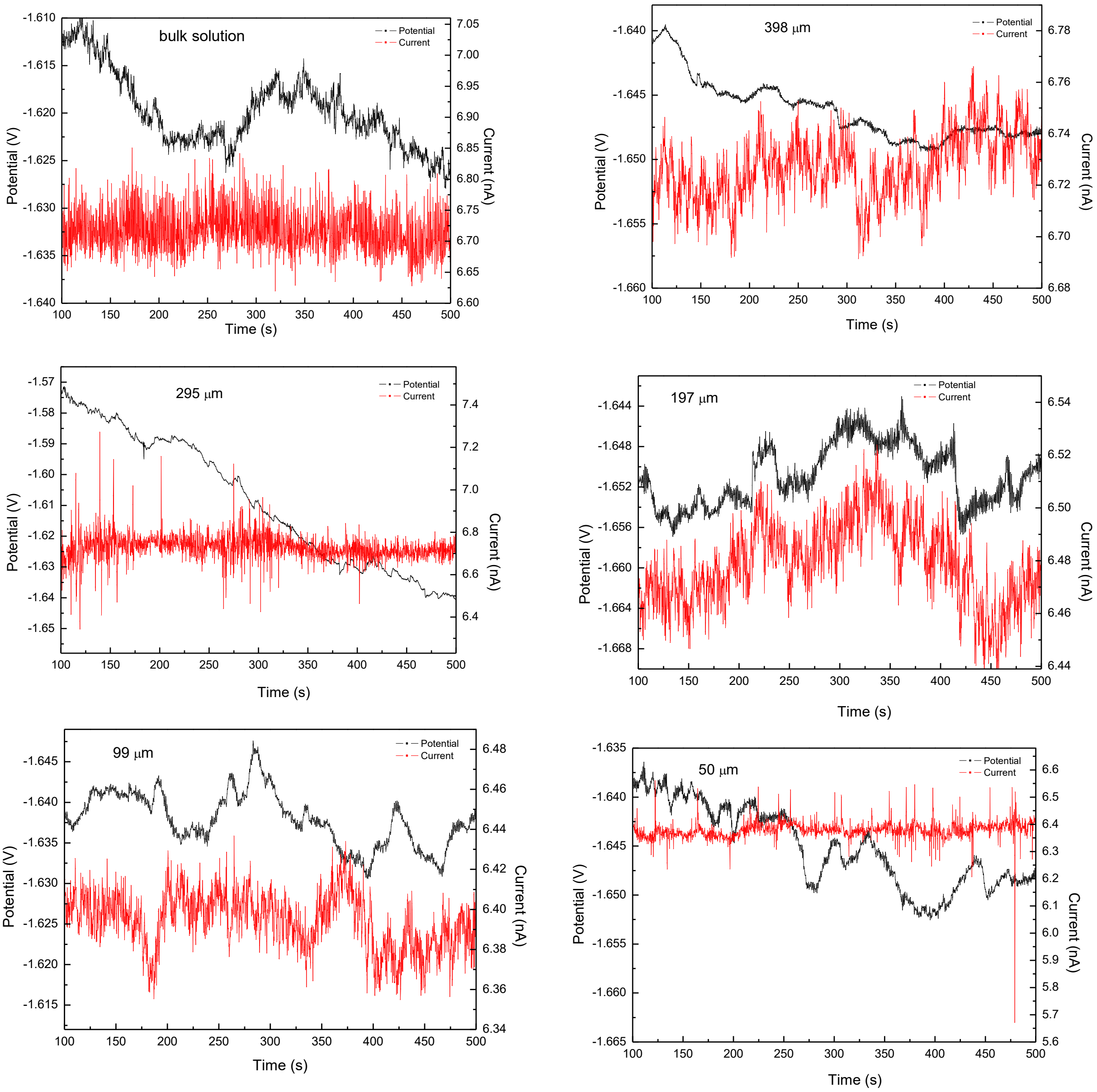

Figure 7. Electrochemical potential and current fluctuations for ZE41 under bulk solution and given thickness of TEL after initial 100 s immersion.

The potential and current noise signals in bulk solution and under different TELs after immersing time of initial 100 s are displayed in Fig. 7. The mean value of the current noise gradually decreases, meanwhile the transient variation is more frequent and drastic with the thinning of the electrolyte layers. For instance, under the TELs of 50 μm, the variation value of the current at a certain point even reaches 0.7 nA and the value of the current in bulk solution is only around 6.7 nA which gradually decreases to 6.4 nA (under the TELs of 50 μm). The result means that the thinning of the TELs can promote the initiation but restrain the development of metastable pitting at the incubation stage and the corrosion resistance of ZE41 increases, which is accordant to the results of the cathodic curves and EIS data. Through potential and current noise signal can reflect the corrosion behavior to some extent, there still lacking quantitative data to character a certain corrosion behavior such as corrosion resistance, metastable pitting, etc. Thus, it is necessary to conduct further frequency domain analysis, which is more powerful than time domain analysis to some extent.

3.2.1 Wavelet analysis of electrochemical noise

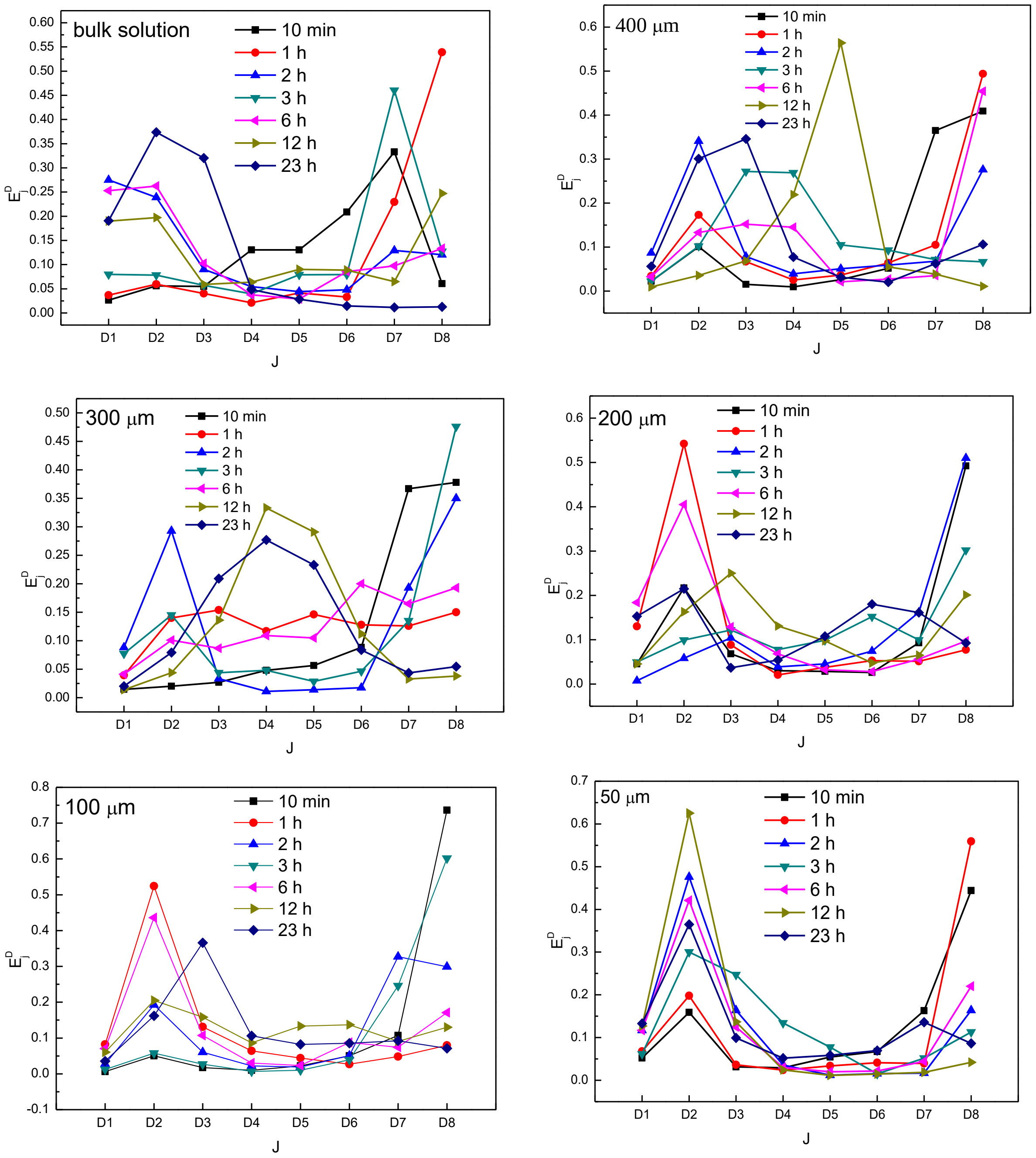

Figure 8. Relative energy distribution plots of the detail coefficient set, D_1, D_2 . . . D_j (the energy is normalized) corresponding to the potential noise signal.

For the electrochemical corrosion process of metal/solution interface, the initiation, development and disappear are quicker than other local corrosion behaviors and are much quicker than the diffusion of corrosive particles, the migration of corrosion products, the evolution of gas and etc., furthermore, the energy distribution of D series cell could reflect the initiation, repassivation and grow processes of corrosion system [28,29]. The study of Li believes that in corrosion system big time constant corresponds to the even dissolution or corrosion process [30]. Homborg proposed that the fine scale coefficients (mainly D_2 and D_3) relate to the activation-controlled process such as metastable pitting, the moderate scale coefficients (D_4-D_6) represent mixture-controlled process (localized corrosion), the big scale coefficients (D_7 and D_8) provide the information of diffusion-controlled process (uniform corrosion) [31,32].

Fig. 8 shows energy distribution plots of the detail coefficient set, D_1, $D_2 \dots D_j$ (the energy is normalized) corresponding to the potential noise signal of ZE41 in bulk solution and under different TELs at various immersion times. It is known that in bulk solution the energy of the wavelet coefficients transfers gradually from the big scale coefficients to the fine scale coefficients (with some fluctuation) along with the corrosion, which indicates that in bulk solution uniform corrosion occurs first, then metastable pitting appears with immersion time. Under the TELs of 400 and 300 μm, the energy mainly concentrates in the coefficient of D_8 at the immersion moment of 10 min and with the immersion time over 6 h the relative energy of D_2-D_5 increases. The relative energy distribution under TELs of 400 and 300 μm suggests that the proportion of metastable pitting increases gradually. Under the TELs of 200 and 100 μm thickness, the change rule of relative energy distribution is similar. In details, after immersion 10 min, the maximal relative energy dominates in the coefficient of D_8, which may correspond to the uniform dissolve of the oxidation film formed in air. With the immersion time of 1 h, the relative energy in D_2 is the largest indicating that the rupture of the passivation film, initiation of metastable pitting and repassivation are the main corrosion process. Whereafter, relative energy fluctuates between big scale coefficients and fine scale coefficients suggesting the competition between the dissolution of the passive film and the initiation of the metastable pitting. At the immersion time of 3 h, the relative energy is outstanding in D_2 and D_3 manifesting the initiation probability increases due to the more exposed of the matrix to the corrosive environment. Under the TELs of 50 μm, the relative energy dominants in D_2 except for the immersion of 10 min to 1 h in D_8, which means under very thin electrolyte layer localized corrosion is the main corrosion form. Through the analysis of EDPs of potential noise, it is clear that in bulk solution, uniform corrosion occurs first and then localized corrosion behavior appears, however, under the TELs metastable pitting which appears at earlier time and increases in proportion with the thinning of the TELs and the increasing of corrosion time is the main corrosion form.

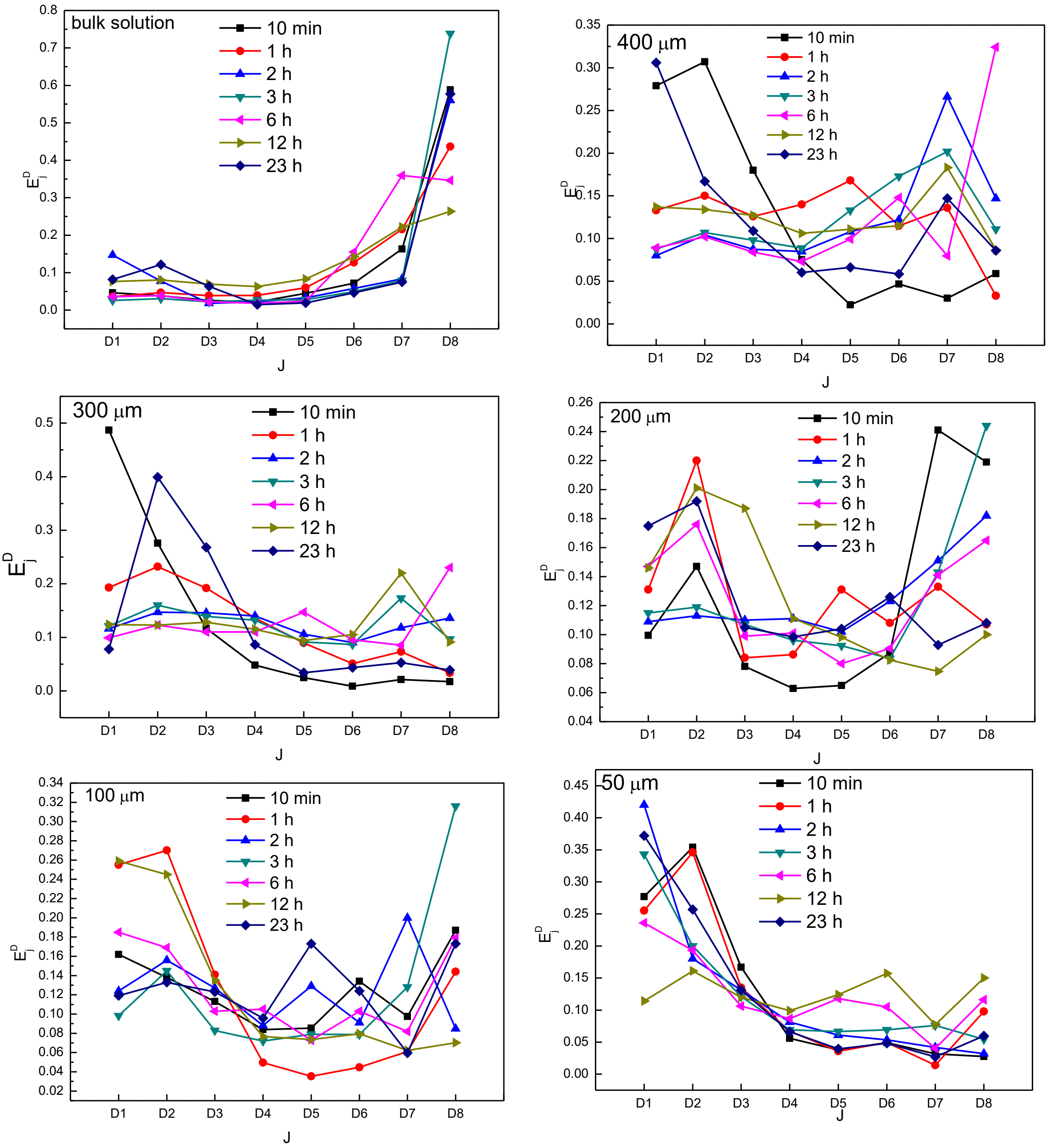

Figure 9. Relative energy distribution plots of the detail coefficient set, D_1, D_2 . . . D_j (the energy is normalized) corresponding to the current noise signal.

Relative energy distribution plots of the detail coefficient set, D_1, D_2 . . . D_j (the energy is normalized) corresponding to the current noise signal (Fig. 9) shows uniform corrosion predominates with relative energy concentrates in D_7 and D_8 [29,33]. With the thickness of TELs changing, the relative energy distribution changes. Under the TEL of 400 μm, according to the relative energy distribution trend the corrosion type can be divided into two phases: firstly, during the time from 10 min to 6 h, the maximal relative energy is in D_2 with the relative energy sum of D_1-D_3 occupy 76.6% at the immersion time of 10 min. With the immersion time to 6 h, the relative energy in D_8 dominates, then the relative energy gathers to fine scale coefficients (6-23 h) and reaches maximum value in D_1 after immersing 23 h. Compared to the TELs of 400 μm, the relative energy distribution under that of 300 μm is similar. It can be suggested that under the TELs of 400 and 300 μm, fast reaction such as the rupture of surface passivation membrane, the initiation of metastable pitting and passivation dominates at initial time, with immersion time uniform corrosion becomes the main process due to the corrosion product film on the electrode surface slowing down the diffusion of corrosion products and Cl^- and then with the further increase of immersion time metastable pitting arises again because of the fracture of surface film under the erosion of Cl^- [34]. Under the TELs of 200 and 100 μm, during the time of 10 min to 3 h the relative energy mainly distributes in D_7 or D_8 (except for the immersion time of 1 h, the energy in D_2 is outstanding). The relative energy in fine scale coefficients is outstanding with the soaking time. For instance, the biggest relative energy domains in D_2 at the immersion time of 6 h, 12 h, and 23 h. Under the TEL of 100 μm, the relative energy distribution is the same to that of 200 μm TELs. The cathodic curves and EIS results manifest that for the TELs thickness thinner than 200 μm the corrosion rate is very small. Combining with the electrochemical noise data it is known that at initial stage of immersion (10 min) the even dissolve of oxidation film formed in air dominates, during the immersion of 10 min to 6 h the initiation, growth and repassivation of metastable pitting compete [30], and then with the time the matrix expose to the corrosive solution directly due to the dissolve of surface film on metal, which means the fast process is primary. Forthermore, at most immersion time the energy concentrates in fine scale coefficients compared to the TELs of 400 and 300 μm, which suggests the proportion of metastable pitting increases with the thinning of the TEL. Under the thickness of 50 μm, the maximal relative energy all distributed in D_1 or D_2 at all the immersion time and the energy of D_1-D_3 occupies about 70 % of the total relative energy. The result means that the fast process such as the initiation and disappearance of metastable pitting or pitting domains under the thickness of 50μm [31,32]. The analysis of EDPs results for current noise shows that in bulk solution uniform corrosion happens, meanwhile under TELs metastable pitting is the primary corrosion type. While under the TELs, metastable pitting arises and the percentage of it increases with the thinning of the TELs thickness and the extension of corrosion time.

From the analysis of the EDPs results of potential and current noise, the obtained conclusion shows a little different. For instance, for the result in bulk solution the EDPs of potential noise illustrate localized corrosion also happens with immersion time, while that of current noise suggests that uniform corrosion dominates during immersion time. The difference may be due to the nature difference of potential and current noise measure through ZRA test system. Fig. 10 shows the schematic diagram of the electrochemical current and potential noise monitoring, in which Z_1 and Z_2 respect the impedance of working and counter electrode respectively and R_s is on behalf of solution resistance between the electrodes. It is clear from Fig. 10 that the potential noise measured is the potential difference between the working and reference electrode. When pitting happens on working electrode, the current produced (i_1) can be divided to two parts, part of which (i_1-$\triangle I$) flow to the cathodic region nearby the corrosion pit, the other part of which ($\triangle I$) flow to counter electrode and is measured by ZRA. The measured current noise can be calculated by Ohm's law ($\Delta I = \frac{Z_1}{Z_1 + Z_2 + R_S} i_1 - \frac{Z_2}{Z_1 + Z_2 + R_S} i_2$). Through the schematic diagram, the measured current noise (ΔI) is just a part of the current produced in localized corrosion. Therefore, in the current research the EDPs results of potential noise are primary.

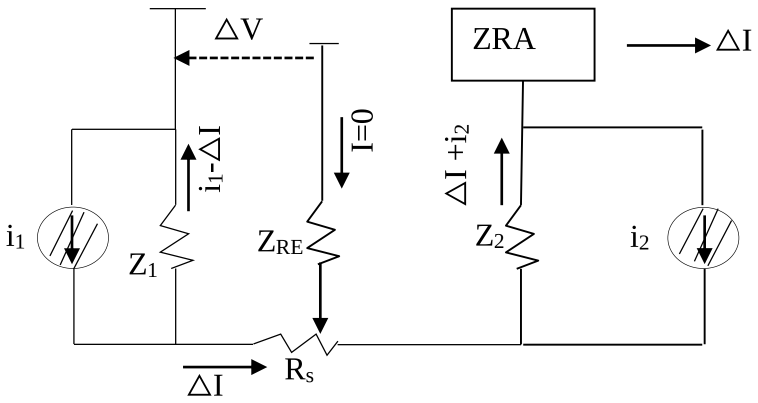

Figure 10. Schematic diagram of the electrochemical noise monitoring [35].

3.2.2 Average electrochemical noise resistance

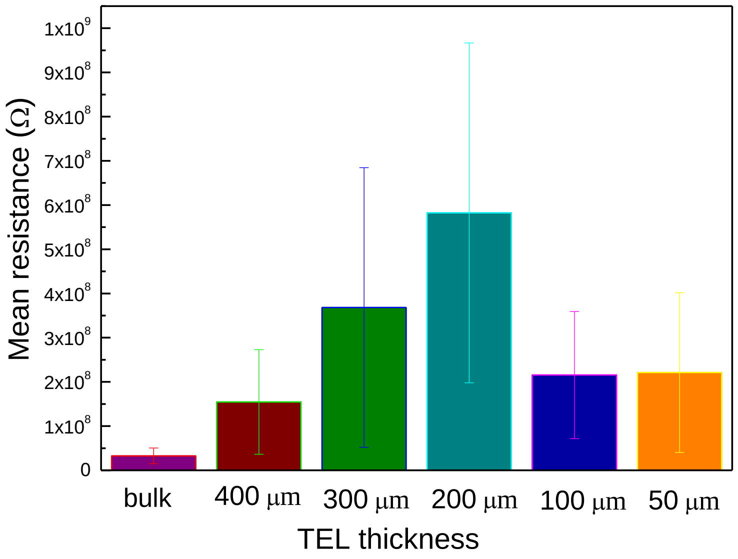

Figure 11. Average electrochemical noise resistance values for the corrosion of ZE41 under given TEL thickness during the exposure time of 24 h.

Fig. 11 shows the average noise resistance values and its standard deviation for the corrosion of ZE41 under given TEL thickness and bulk solution during the exposure time of 24 h. The standard deviation value reflects the dispersion degree of the noise resistance during the immersion time of 24 h. Some studies indicate that noise resistance is inversely proportional to corrosion activity [36,37,38]. It is known from Fig. 11 that average noise resistance values and the standard deviation values under the TELs are apparently higher than that in bulk solution, which indicates that the corrosion resistance increases and the fluctuation of corrosion resistance is violent under TELs. Also, it is clear that the corrosion resistance under the thickness of 200 μm is maximal, which shows a little difference from the results of cathodic curves and EIS mentioned above. The difference maybe the cathodic curves and EIS results reflect the overall information of the corrosion electrode, while electrochemical noise results mainly reflect the localized information. It is also known from discrete wavelet transform that localized corrosion such as metastable pitting is the primary corrosion type, which indicates that electrochemical noise possesses better resolution for monitoring localized corrosion, while cathodic curves and EIS shows better effect for uniform corrosion.

4. CONCLUSION

The current study shows no matter in bulk solution or under the TELs, the cathodic process of magnesium alloy ZE41 is controlled by the reduction of hydronium ion. The cathodic polarization curves indicate that under the TELs the diffusion process is restrained, which results in both the inhibition of cathodic and anodic processes. In details, under the TELs the reduce of the concentration of H_3O^+ the cathodic process needed and the corrosion product film on the metal surface due to the increase of localized alkalinity. So the corrosion resistance of ZE41 under the TELs is enhanced, which is in accordance to the EIS results. The EDPs of potential noise of ZE41 shows the information that in bulk solution uniform corrosion preferentially occurs and with the immersion time localized corrosion also arises, while under the TELs metastable pitting and other localized corrosion occupies higher ratio and with the thinning of the TELs and increasing of immersing time the ratio becomes higher. That is to say under the TELs localized corrosion is the prime corrosion type. The result is in agreement to the more severe of the fluctuation of corrosion resistance in EIS.

Moreover, the corrosion rate information reflected by noise resistance shows different to the result of EIS and cathodic curves. The difference can be explained that cathodic curves and EIS mainly reflect the overall information, while the electrochemical noise focuses more on localized corrosion. Meanwhile, from the analysis of EDPs it is known that under the TELs localized corrosion is the main corrosion type, so the results have certain deviation.

DISCLOSURE STATEMENT
No potential conflict of interest was reported by the author(s).

ACKNOWLEDGEMENT
This work was supported by National Key R&D Program of China (No. 2017YFB0702802), National Natural Science Foundation of China (No. 51771174), and the National Environmental Corrosion Platform.

References

1. C. Zhong, F. Liu, Y. T. Wu, J. J. Le, L. Liu, M. F. He, , J. C. Zhu and W. B. Hu, *J Alloy Compd*. 520 (2012) 11.
2. P. Dauphin-Ducharme, J. Mauzeroll, *Anal Chem*. 87 (2015) 7499.
3. M. Esmaily, D. B. Blucher, R. W. Lindstrom, J. E. Svensson and L. G. Johansson, *J Electrochem Soc.* 162 (2015) C260.
4. H. L. Ho, S. H. Hsiang and Y. H. Fan, *J Chin. Soc. Mech. Eng*. 35 (2014) 67.
5. G. Baril, , and Pébère, N., *Corros Sci*. 43 (2011) 471.
6. A. Dhanapal, S. Rajendraboopathy, V. Balasubramaninian, S. R. Rao and A. R. Zaman, *Corros. Eng .Sci. Techn.* 47 (2012) 425
7. M.C. Merino, A. Pardo, R. Arrabal, S. Merino, P. Casajús and M. Mohedano, *Corros. Sci*. 2010; 52: 1696-1704.
8. L. Wang, T. Shinohara, B. P. Zhang and H. Iwai, *J. Alloy Compd.* 485 (2009) 747.
9. Z. Y. Cui, X. G. Li, K. Xiao, *Corros. Eng. Sci. Techn*. 49 (2014) 363
10. W. J. Liu, F. H. Cao, A. N. Chen, L. R. Chang, J. Q. Zhang and C. N. Cao,. *Corros. Sci.* 52 (2010) 627.
11. Y. L. Cheng, Z. Zhang, F. H. Cao, J. F. Li, J. Q. Zhang, J. M. Wang and C. N. Cao,. *Corros. Sci*. 46 (2004) 1649.
12. S. Johnston, Z.M. Shi and A. Atrens, *Corros. Sci*. 101 (2015) 182.
13. C. Taltavull, Z.M. Shi, B. Torres, J. Rams and A. Atrens, *J. Mater. Sci. Mater. Med*. 25 (2015) 329.
14. P. Chakraborty Banerjee, R. K. Singh Raman, Y. Durandet and G. McAdam, *Corros. Sci*. 53 (2011) 1505.
15. L. L. Nie, Y. Xia, Y. R. Zhou, J. X. Zhang, F. H. Cao, and J. X. Zhang, *Int. J. Electrochem. Sci*. 11 (2016) 259
16. A. Dhanapal, S. Rajendra Boopathy, and V. Balasubramanian, *J. Alloy Compd*. 523 (2012) 49.
17. K. Gusieva, C. H. J. Davies, J. R. Scully and N. Birbilis, *Int. Mater. Rev*. 60 2015) 169.
18. M. Jamesh, S. Kumar and T. S. N. Sankara Narayanan, *Corros. Sci*. 53 (2011) 645.
19. M. Mosiałek, G. Mordarski, P. Nowak, W. Simka, G. Nawrat, M. Hanke, R. P. Socha and J. Michalska, *Surf. Coat. Tech*. 206 (2011) 51.
20. Y. Xin, C. Liu, W. Zhang, K. Huo, G. Tang, X. Tian and P. K. Chu, *J. Mater. Res*. 23 (20111) 312.
21. G. Song and K. A. Unocic, *Corros. Sci*. 98 (2015) 758.
22. C. M. A. Brett, L. Dias, B. Trindade, R. Fischer and S. Mies, *Electrochim. Acta.* 51 (2006) 1752.
23. Y. G. Li, Y. H. Wei, L. F. Hou and P. J. Han, *Corros. Sci*. 69 (2013) 67.
24. R. A. Cottis, A. M. Homborg and J. M. C. Mol, *Electrochim. Acta*. 202 (2016) 277.
25. R. A. Cottis, Corrosion. 57 (2011) 265.
26. A. Aballe, M. Bethencourt, F. J. Botana and M. Marcos, *Revista De Metalurgia*. 35(6) (1999) 384.
27. A. Aballe, M. Bethencourt, F. J. Botana and M. Marcos, *Electrochem. Commun*. 1 (1999) 266.
28. C. Cai, Z. Zhang, F. H. Cao, Z. Gao, J. Q. Zhang and C. N. Cao, *J. Electroanal. Chem*. 578 (2005) 143.
29. F. H. Cao, Z. Zhang, J. X. Su, Y. Y. Shi and J. Q. Zhang, *Electrochim. Acta*. 51 (2006) 1359.
30. Y. Li, R. G. Hu, J. R. Wang, Y. X. Huang and C. J. Lin, *Electrochim. Acta*. 54 (2009) 7134.
31. R. Moshrefi, M. G. Mahjani and M. Jafarian, *Electrochem. Commun.* 48 (2014) 49.
32. A.M. Homborg, T. Tinga, X. Zhang, E. P. M. Van Westing, P. J. Oonincx, J. H. W. de Wit and J. M. C. Mol, *Electrochim. Acta*. 70 (2012) 199.
33. A. Aballe, M. Bethencourt, F. J.Botana, M. Marcos and R. M. Osuna, *Electrochim. Acta*. 47 (2002) 1415.
34. T. Zhang, Y. W. Shao, G. Z. Meng and F. H. Wang, *Electrochim. Acta*. 53 (2007) 561.
35. A. Aballe and F. Huet, *J. Electrochem. Soc.* 149 (2002) B89.
36. P. Casajús and N. Winzer, *Corros. Sci*. 94 (2015) 316.

37. T. Zhang, C. M. Chen, Y. W. Shao, G. Z. Meng, F. H. Wang, X. G. Li and C. F. Dong, *Electrochim. Acta.* 53 (2008) 7921.
38. A. N. Chen, F. H. Cao, X. N. Liao, W. J. Liu, L. Y. Zheng, J. Q. Zhang and C. N. Cao, *Corros. Sci.* 66 (2013) 183.